JOURNAL OF RAMAN SPECTROSCOPY
J. Raman Spectrosc. 2002; **33**: 165–172
Published online in Wiley InterScience (www.interscience.wiley.com). DOI: 10.1002/jrs.814

JRS

Raman mapping in the elucidation of solid salt eutectic and near eutectic structures†

Rolf W. Berg* and David H. Kerridge

Department of Chemistry, DTU Building 207, Technical University of Denmark, Kemitorvet, DK-2800 Kgs. Lyngby, Denmark

Received 31 August 2001; Accepted 20 October 2001

The distribution of the different components of solidified eutectic or near-eutectic salt mixtures (eutectics) was examined by use of Raman microscope mapping of the structures formed when these melts were slowly cooled. Seven binary and one ternary system were investigated. In most cases the component crystallized phases consisted of roughly rounded areas of about 0.5–5 μm across, the areas alternating in all directions across the sections. These three-dimensional structures may best be described by the term 'conglomerate.' The size of these areas depended on the cooling rate and the composition. When unidirectional cooling was applied it was possible for the system ($KCl–Na_2SO_4$, 60 : 40 mol/mol) to observe lamellar arrangements of the component phases, in an arrangement closely similar to what is frequently found among metallic or ceramic eutectics. Each area, conglomerate or lamellar, did not consist of a pure chemical component, although having one component in a high concentration. Probably the behaviour represents separation on solidification due to the limiting solid solubility. The 'conglomerate' structures are very different from what has been found for metallic or ceramic eutectics. Small changes in composition, in sectioning direction and in solidification technique were found to result in relatively small differences. The major effect was found to result from the rate of solidification, faster cooling causing markedly smaller rounded areas with the 'conglomerate' becoming much finer grained. The high area of 'interphasial' contact between the solid solutions is considered to be responsible for the unexpectedly high electrical conductivity previously found and to give rise to part of the melting enthalpy differences between those of solidified salt eutectics and those of the corresponding unmelted mechanical mixtures of the component salts. Mixtures with a larger variation away from the eutectic composition also showed a 'conglomerate' structure, but with bigger and more irregular areas. Copyright © 2002 John Wiley & Sons, Ltd.

INTRODUCTION

A recent extension of Raman spectroscopy has been to utilize an optical microscope with a moving table to establish the composition variation over a chosen area, so-called Raman mapping. In the present work this technique was applied to the spatial distribution of phases when a molten homogeneous two-component salt eutectic or near-eutectic (salt A + salt B) is frozen. The phase diagram then usually indicates the formation on freezing of two solid phases (a solid solution of B in A, and one of A in B, often referred to as α and β solid solutions, respectively).

The study of analogous systems composed of two metallic components has been in progress for many years and many structures have been reported. In contrast the structures of solidified salt mixtures have not been studied until recently, despite the fact that the chemistry of molten salt eutectics has been the object of a large volume of research. Though solidified salts do not have the practical importance of lamellar metallic structures (for example, the working temperatures and thus the efficiency, of gas turbine blades can be increased by arranging growth of lamellae parallel to the blade surface), recent measurements of electrical conductivity[1,2] and melting enthalpies[3,4] have indicated a large amount of interfacial contact between two-component solid salt solutions.

Metallurgists and ceramists have devoted great efforts to understanding the structures and spatial arrangement(s) of their eutectics and have frequently reported rapidly alternating phases of lamellar or fibrous forms. However, salt structures cannot be studied as readily as, e.g., those of metallic eutectics, for whereas many suitable etches are known which differentiate between the metallic phases, in the case of salts most liquids (potential etches) attack and dissolve both phases, thus destroying the planar surfaces produced by grinding and polishing, and complicating the analysis of the magnified optical image.

*Correspondence to: R. W. Berg, Department of Chemistry, DTU Building 207, Technical University of Denmark, Kemitorvet, DK-2800 Kgs. Lyngby, Denmark. E-mail: rwb@kemi.dtu.dk
†Dedicated to the Memory of the Late Professor Murray Brooker, of Memorial University, Newfoundland, Canada.

JRS

Table 1. Raman spectral characteristics[a] of anions[5,6]

Unperturbed ion	Symmetry	Raman-active fundamentals			
Cl^-, Br^-	Spherical	no			
Nitrite, NO_2^-	Non-linear, C_{2v}	$\nu_1(A_1)$ ~1330 cm^{-1}	$\nu_2(A_1)$ ~810 cm^{-1}	$\nu_3(B_2)$ ~1250 cm^{-1}	
Nitrate, NO_3^-	Triangular planar, D_{3h}	$\nu_1(A_1')$ ~1050–1070 cm^{-1}	Only active in IR $\nu_2(A_2'')$ ~830 cm^{-1}	$\nu_3(E')$ ~1380 cm^{-1}	$\nu_4(E')$ ~715 cm^{-1}
Sulfate, SO_4^{2-}	Tetrahedral, T_d	$\nu_1(A_1)$ ~985 cm^{-1}	$\nu_2(E)$ ~450 cm^{-1}	$\nu_3(F_2)$ ~1105 cm^{-1}	$\nu_4(F_2)$ ~610 cm^{-1}

[a] The band positions depend somewhat on the crystal phase and kind of cation; see, e.g., data on nitrates.[7–9]

In the present work, it has now been found for many solidified salt eutectics that Raman mapping can conveniently distinguish between the two solid solutions in the planar surface, and that technique can thus give information on the three-dimensional structure. Since the method depends on the presence of Raman signals, its only essential limitation is dependent on the choice of salt anions or cations. Hence a Raman-active mode must be present in at least one of the phases. Conventionally, both (all if ternary or higher eutectics are considered) components have Raman-active bands. However, during this work it was found that adequate mapping of a binary eutectic can be obtained with only one component having a Raman-active band. Raman characteristics of the salts studied are given in Table 1.

The principle of confocal Raman microscopy (mapping) is based on the automatic successive recording of Raman spectra from many spots on a flat sample surface by use of a motorized X–Y microscope table, and from these spectra a two-dimensional Raman map is computed, based on band intensities in specific wavelength intervals.[10]

The Raman mapping method is particularly well suited to identifying the eutectic structures formed with oxyanion compounds, since they often give Raman bands with characteristic positions and conveniently high intensities. Strong Raman lines allow short accummulation times, e.g. of a few seconds per spot examined, and hence the measurement of many spots across a surface within a reasonable time. Modern software allow repeated recordings, averaging and automatic removal of cosmic events.

Eight low and somewhat higher melting eutectic salt samples were prepared, sectioned, ground, polished and examined by Raman microscopy.

EXPERIMENTAL

Samples

The eutectics examined and their melting points are given in Table 2. The compounds used for their preparation were of pro analysi quality, dried, weighed out in the specified proportions, ground together and melted in 10 mm i.d. Pyrex tubes with either rounded ends or drawn out to a point at their lower ends. Heating and cooling operations took place either in a static electronically controlled very slowly cooled furnace (rate 1 or 0.1 °C h^{-1}) or by controlled slow extrusion into ambient temperature (rate 5 mm h^{-1}) from an isothermal furnace, in some cases in the former with a massive aluminium block wired to the lower end, reaching partly outside the isothermal section so as to provide a thermal gradient. Visual inspection showed that the molten eutectics initially solidified to transparent/translucent solids, which turned white and opaque on further cooling, a feature possibly due to differential thermal contraction and/or to phase changes. The glass tube was broken and the rod-shaped solidified eutectic was cut in a specified direction and ground with paraffin on a metallurgical polishing machine with, successively, P220 and 1200 carborundum papers and finally with a lap impregnated with 0.25 μm diamond paste. The best results were obtained when lubricating with paraffin and washing off with n-pentane. Other lubricants (ethylene glycol, water) and washing liquids (acetone) were tried but resulted in dissolution of more of the salt surface. The measurements were taken on polished salt surfaces cut at 90, 45 or 0° to the cylindrical axis of the specimen. Alternatively, the solidified surface was found to be sufficiently flat that it could sometimes be used without further preparation.

Table 2. Eutectic salt mixtures studied and their melting-points

Eutectic mixture	Composition (mol%)	Melting-point (°C)
$NaNO_2$–$NaNO_3$	59 : 41	227
KNO_2–KNO_3	24 : 76	315
$NaNO_3$–KNO_3	50 : 50	220
KNO_3–$Ca(NO_3)_2$	65.8 : 34.2	145
$NaNO_2$–$NaNO_3$–KNO_3	48.9 : 6.9 : 44.2	142
NaBr–$NaNO_3$	9.5 : 90.5	293
KCl–$K_2Cr_2O_7$	25 : 75	368
KCl–K_2SO_4	60 : 40	520

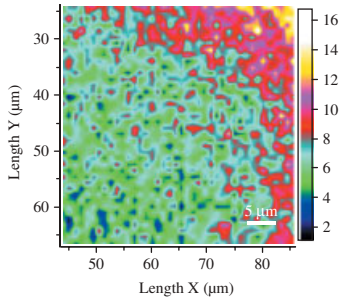

Figure 1(B)

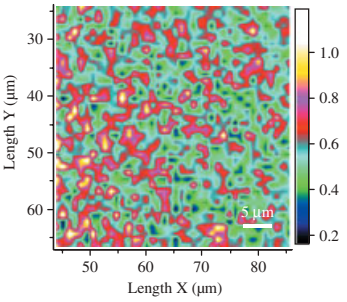

Figure 1(C)

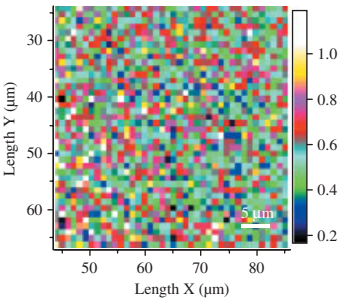

Figure 1(D)

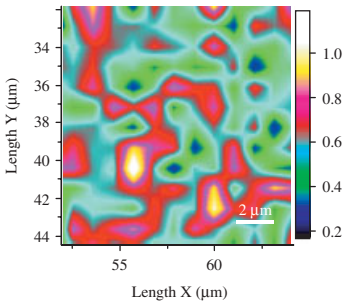

Figure 1(E)

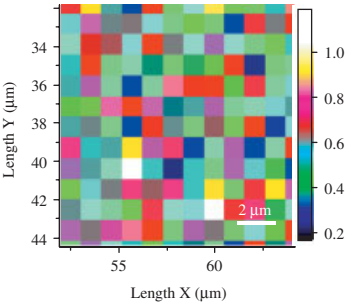

Figure 1(F)

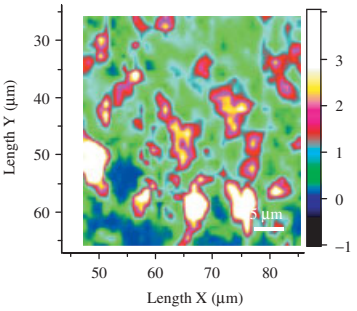

Figure 2(B)

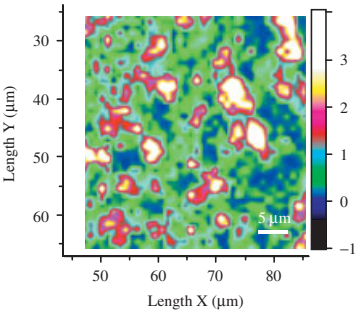

Figure 2(C)

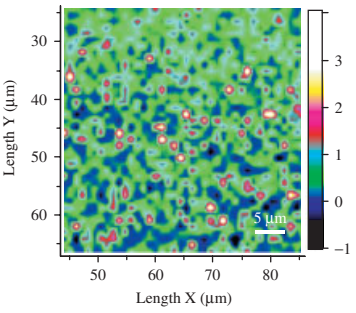

Figure 3(B)

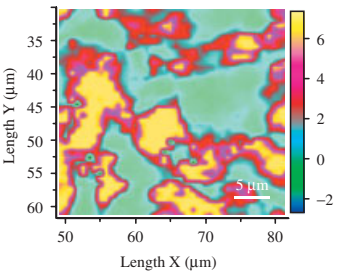

Figure 4(B)

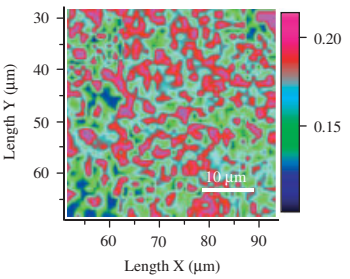

Figure 5(B)

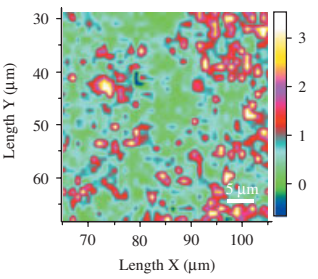

Figure 6(A)

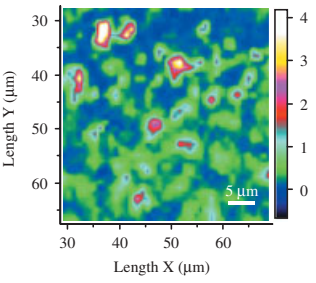

Figure 7(A)

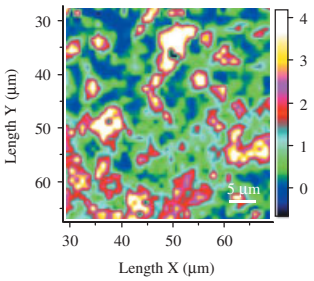

Figure 7(B)

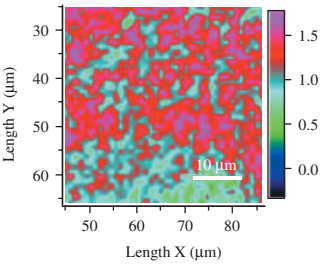

Figure 8(B)

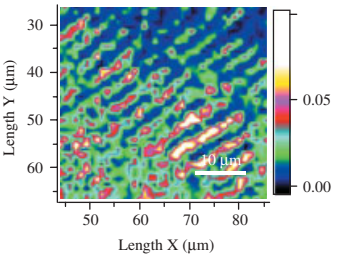

Figure 9(B)

Plate 1

Mapping

A DILOR XY Raman spectrometer with microscope entrance was used for the measurements. Excitation was with filtered green laser radiation having a wavelength of 514.5 nm (argon ion laser) or 532 nm ($Nd-YVO_4$ laser) at a power of about 0.2–1 W and with vertical polarization. The Rayleigh/laser line was filtered off by use of Kaiser holographic SuperNotch-Plus filters (cut-offs ~100–200 cm^{-1}). The Raman light was dispersed on to a CCD detector (operated at 140 K) by use of either an 800 mm focal length single spectrograph with an 1800 lines mm^{-1} grating, or by use of a second spectrograph with a much shorter focal length and a grating with 600 lines mm^{-1}. In both cases the slit widths were set to 100 μm, corresponding to a spectral resolution of about 4–5 cm^{-1}. A sheet polaroid analyser, which permitted vertically or horizontally polarized light to pass followed by a quarter-wave depolarizer, was used to check the polarization data. Calibration of the wavenumber scales to an accuracy of ±1 cm^{-1} was done with neon lines superimposed on the spectra; otherwise calibration errors as large as 30 cm^{-1} were sometimes obtained with the second monochromator (R. W. Berg and T. Nørbygaard, personal communication). The microscope table was controlled by the DILOR Labspec program. The spot size, unless specified otherwise, was set to 1 μm by use of a 100× objective and a 180 μm confocal hole. For each picture, Raman spectra of 40 × 40 spots were normally used. Spectral and image files were collected as .tsf and .tvf format files fitting the same software. Raman band areas over the background (in counts times wavenumber range) were automatically calculated employing built-in baseline correction procedures without any smoothing. The mappings were based on the ratio between one band area and another band area within the same spectrum, because instabilities in the set-up were largely compensated in that way: a spot that is slightly out of focus because of the sample is not entirely flat (or not entirely parallel with the *XY* plane) will give a spectrum with reduced intensity, but the ratio will still be approximately correct. The same applies to, e.g., intensity variations in the laser output. The mappings were smoothed from spot to spot for both the *X* and the *Y* directions, allowing the eye to appreciate the revealed structures more easily. Addition of an artificial colour scale also made the structural distribution clearer. The relative concentrations of the chemical components were estimated from measurement of chosen lines averaged over 40 × 40 μm areas of prepared standard solid mixtures of 90:10, 50:50 and 10:90 mol%. Other experimental details are given in the figure captions or have been given previously.[11]

RESULTS AND DISCUSSION

$NaNO_2-NaNO_3$ system

Typical results for the $NaNO_2-NaNO_3$ system are shown in Figs 1–4. Raman mapping of its eutectic composition

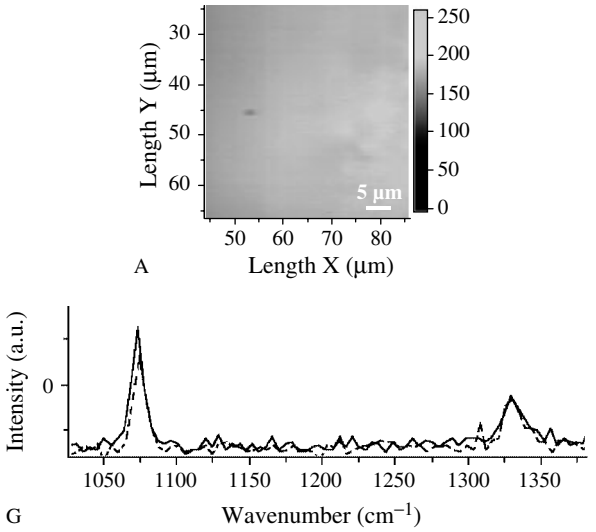

Figure 1. Standard optical microscope picture (A) and Raman mappings (B–F) of 50:50 molar ratio $NaNO_2-NaNO_3$ mixture, melted and solidified in a stationary furnace at a cooling rate of 10 °C h^{-1}. Raman spectra were determined directly on the unground cylindrical surface. (B) shows a mapping, based on the intensity of the ~1329 cm^{-1} $NaNO_2$ band in the range 1300–1360 cm^{-1}. (C) shows a ratio mapping based on the same data but plotting the $NaNO_2$ band relative to the ~1068 cm^{-1} $NaNO_3$ band intensity, integrated from 1040 to 1110 cm^{-1}. The effect of smoothing is illustrated in (D), which shows an unsmoothed version of (C). Enlargements of mappings (C) and (D) are shown in (E) and (F). Examples of spectra obtained in a dark blue area (solid curve, high in $NaNO_3$) and in a white to yellow area (dashed curve, high in $NaNO_2$) are given in (G) for points at {62, 35} and {56, 41}, respectively, excited with 800 mW of 532 nm laser radiation, each spot exposed twice for 1 s, averaged and cosmic-ray spikes removed. Note: the Raman spectral abscissa not calibrated. For parts (B)–(F), see plate 1.

have already been reported.[11] Under the optical microscope the samples were featureless. However, as seen in, e.g., Figs 1(C), 2(B), 3(B) and 4(B), informative Raman mappings can be made on the basis of the suitably strong and distinctive Raman signals of the nitrite and nitrate anions. It was possible, even when the differences were small as in the two examples of spectra in Fig. 1(G), to determine mappings with many features and in particular in this way to help understand the effect of crystallization conditions, method and rate of cooling, tube shape and size, etc. We were able to show clearly the structure of the near-eutectic solidified $NaNO_2-NaNO_3$ mixtures and show that there was considerable segregation of the NO_2^- and NO_3^- components.

Because of the sensitivity of the focus adjustment at the high microscope magnification of 100× and a general lack of flatness on the micrometer scale, the Raman signal

JRS

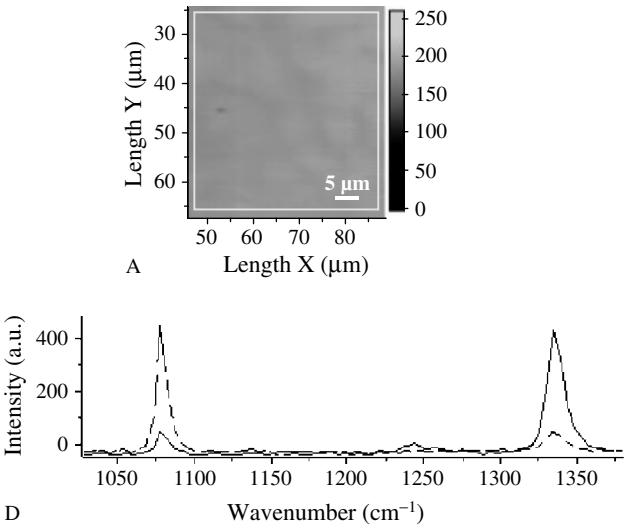

Figure 2. Standard optical microscope picture (A) and Raman mappings (B and C) of 56 : 44 molar ratio $NaNO_2$–$NaNO_3$, solidified by pushing at a rate of 5 mm h^{-1}. The Raman mappings shown were determined from spectra taken on a ground and polished section parallel with the sample axis and near the outside surface (B, same place as shown in A) and perpendicularly to the axis (C). The mappings were based on the ratio of the ~1329 cm^{-1} $NaNO_2$ band area (from 1300 to 1360 cm^{-1}) to that the ~1068 cm^{-1} $NaNO_3$ band (from 1040 to 1110 cm^{-1}). Example spectra (abscissa not calibrated) are given in D for a dark blue area (solid curve, high in $NaNO_3$) and for a white to yellow area (dashed curve, high in $NaNO_2$). Experimental details as given in Fig. 1. For parts (B) and (C), see plate 1.

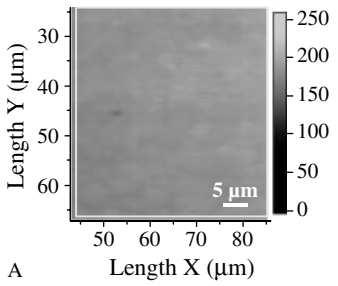

Figure 3. Standard optical microscope picture (A) and Raman mapping (B) of 40 : 60 molar ratio $NaNO_2$–$NaNO_3$ for a ground and polished cross-section perpendicular to the sample axis. The mapping was based on the ratio of the ~1329 cm^{-1} $NaNO_2$ band to the ~1068 cm^{-1} $NaNO_3$ band in the ranges 1300–1360 and 1040–1110 cm^{-1}. Other experimental details as given in Fig. 1. For part (B), see plate 1.

strength varied considerably from spot to spot. Thus, instead of using absolute band areas to compose the mappings, as in Fig. 1(B), it was found that better images could be obtained by using the ratio of selected bands [Fig. 1(C)]. For areas

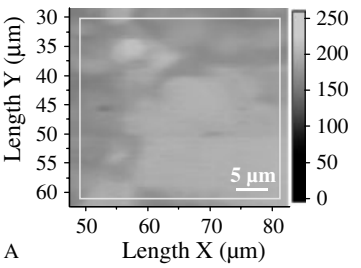

Figure 4. Standard optical microscope picture (A) and Raman mapping (B) of 62 : 38 molar ratio $NaNO_2$–$NaNO_3$. Experimental details as given in Fig. 1. For part (B), see plate 1.

partly out of focus, all bands decreased in the same manner but the ratio between two bands in the same spectrum was invariant to focusing, although subject to noise. The influence of smoothing can be seen by comparing Fig. 1(C) with Fig. 1(D). The sharp edges of the square spots have been removed by the smoothing algorithm. Enlarged details are shown in Fig. 1(E) and (F). Even though the spectra, as in the two examples in Fig. 1(G), do not differ much, an informative mapping can still be obtained.

In Figs 2–4 the slower cooling gave much better Raman spectra and the resulting mappings were better. This was mainly the result of the larger areas of the components, since with smaller areas the 1 μm spot size overlapped relatively more with adjacent areas of different composition in both *X* and *Y*, and also *Z*, directions, resulting in spectra having more signal from adjacent areas; especially the *Z* averaging (depth) is probably important because of the transparency of the samples might result in averaging over a few micrometers.

As mentioned the $NaNO_2$–$NaNO_3$ segregation behaviour can clearly be seen in the mappings [Figs 1(C), 2(B), 2(C) and 3(B)]. Other Raman mappings of other systems gave similar results, showing closely packed, roughly rounded particles. The chemical components were in general gathered into rather irregular, roughly circular, masses, of about 0.5–5 μm across, with compositions ranging, e.g., from high in nitrite to high in nitrate, both with smaller concentrations of the other constituent, and without large areas of approximately equimolar composition. The roughly circular areas seen may perhaps best be described as a 'conglomerate' kind of structure, to adapt a geological term. Ubbelohde in his book *The Molten State of Matter*[12] also used the word 'conglomerate' to describe solid salt eutectics. Separate measurements on the solid single salts and their mixtures showed that the area ratio scales to the right in, e.g., Fig. 1(C), because of different Raman band scattering efficiencies in nitrate and nitrite, should be divided by a factor, perhaps ~1.25, to convert it to concentration ratios. In Fig. 4(B) areas of yellow or blue colour have area ratios of perhaps 7 and 0.15, and a significant separation of NO_2^- and NO_3^- is obvious.

Important parameters for the spatial extent of the observed structures were found to be (i) the rate of cooling, fast rates producing notably smaller 'conglomerates' (e.g. Fig. 1), and (ii) the deviation from the eutectic composition: the more deviation, the coarser and less regular the 'conglomerates' (Figs 2–4). Although the optical microscopy of ground and polished surfaces showed little indication of the structure [Figs 1(A), 2(A), 3(A) and 4(A)], it was apparent that whilst the separation of nitrite and nitrate could be high, the other component was always present, despite the probable overlap of the Raman spot on to adjacent rounded areas. We think that this is a real feature of the eutectics and not due to this instrumental effect because the bigger conglomerates, produced by slower cooling, where this instrumental effect would be less, also showed both components to be present, and in similar ratios. Hence the discrete rounded areas are believed to be the two solid solutions rather than pure compounds. In any case, the phase diagram suggests the eutectic mixture would not freeze into the pure components.

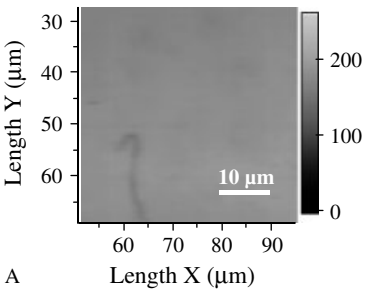

Figure 5. Standard optical microscope picture (A) and Raman mapping (B) of 24 : 76 molar ratio KNO_2–KNO_3, solidified in a stationary furnace at a cooling rate of 0.1 °C h^{-1}. The mapping was determined on a ground and polished surface, cross-section perpendicular to axis, based on 40 × 40 Raman intensity ratios of the KNO_2 band to the KNO_3 band, in the ranges 1255–1360 and 1000–1060 cm^{-1}. For part (B), see plate 1.

Other systems

Similar 'conglomerate' structures, found for the systems of KNO_2–KNO_3 (molar ratio 24 : 76) and $NaNO_3$–KNO_3 (molar ratio 50 : 50) are shown in Figs 5 and 6. The same

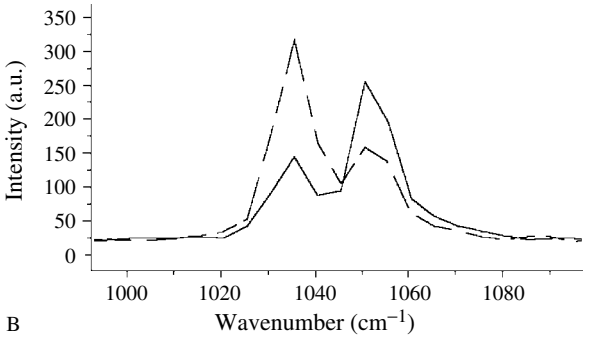

Figure 6. Raman mapping (A) of 50 : 50 molar ratio $NaNO_3$–KNO_3, solidified at a cooling rate of 1 °C h^{-1}. The Raman mapping was obtained on a ground and polished perpendicular cross-section based on $NaNO_3$ and KNO_3 bands at ~1068 and ~1050 cm^{-1}. Characteristic spectra of light yellow area (solid line, mostly $NaNO_3$) and dark blue area (dashed line, mostly KNO_3) are given (B, abscissa not calibrated). Excited with 200 mW of 514.5 nm radiation. For part (A), see plate 1.

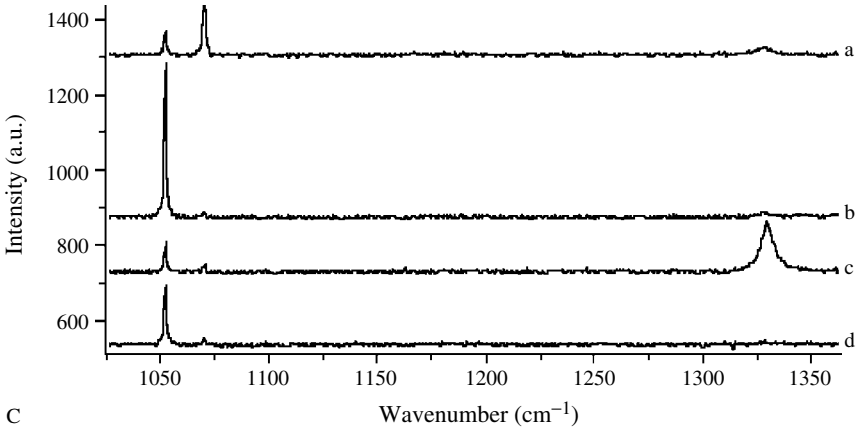

Figure 7. Raman mappings of an $NaNO_2$–$NaNO_3$–KNO_3 mixture of molar ratio 49.8 : 6.9 : 44.2, solidified by pushing at a rate of 5 mm h^{-1}, ground in paraffin and washed with pentane. (A) shows the $NaNO_3$–KNO_3 and (B) the NO_2^-–NO_3^- ratio mappings obtained from the same set of 40 × 40 spectra. Four typical spectra are given in (C) (Abscissa not calibrated), showing from top to bottom high (a), low (b) $NaNO_3$–KNO_3 molar ratios [ranges 1063–1078 and 1046–1060 cm^{-1}, white and dark, respectively in (A)], and high (c), low (d) NO_2^-:NO_3^- molar ratios [ranges 1315–1348 and 1037–1079 cm^{-1}, white and dark, respectively, in (B)]. Bands at ~1055, ~1068 and ~1329 cm^{-1} are due to KNO_3, $NaNO_3$ and (Na/K)NO_2, respectively. Excited with 200 mW of 514.5 nm radiation. For parts (A) and (B), see plate 1.

JRS

kind of results have also been found for the ternary 'heat transfer salt' eutectic, $NaNO_2$–$NaNO_3$–KNO_3 (molar ratio 49.8 : 6.9 : 44.2). In the latter system three Raman signals were collected, enabling two different ratios to be mapped, i.e. $NaNO_3$–KNO_3 and NO_2^-–NO_3^- [Fig. 7(A) and (B)] which showed that the structure was again a 'conglomerate' which now consisted of alternations of all three component solid solutions. There was no change in the conglomerates with longer irradiation times, indicating that the structures were not affected by the kind of radiation and the power level used.

In a further extension of the technique, it was found possible to obtain informative mappings when only one of the components had a Raman signal. An example for the case of NaBr–$NaNO_3$, is shown in Fig. 8. This solidified eutectic again showed a 'conglomerate' structure when the area ratio of the nitrate signal to that of the filtered Rayleigh line was plotted. The ratio was again found of advantage to make some allowance for incomplete flatness (variation in focus) and thus gave better results than when using the anion signal alone. A 'conglomerate' kind of structure was also found when studying the solid KCl–$K_2Cr_2O_7$ eutectic

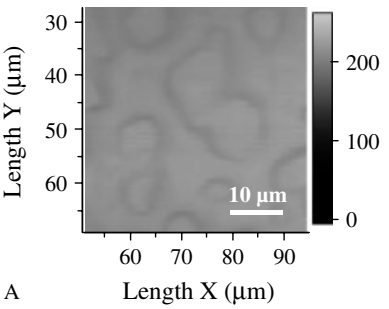

Figure 8. Standard optical microscope picture (A) and Raman mapping (B) of 9.5 : 90.5 molar ratio NaBr–$NaNO_3$. The mapping was based on the $NaNO_3$ band area in the range from 980 to 1200 cm^{-1}, ratioed over the area of the filtered Rayleigh band from −100 to +900 cm^{-1} from a set of 40 × 40 spectra. Excited with 200 mW of 514.5 nm radiation. For part (B), see plate 1.

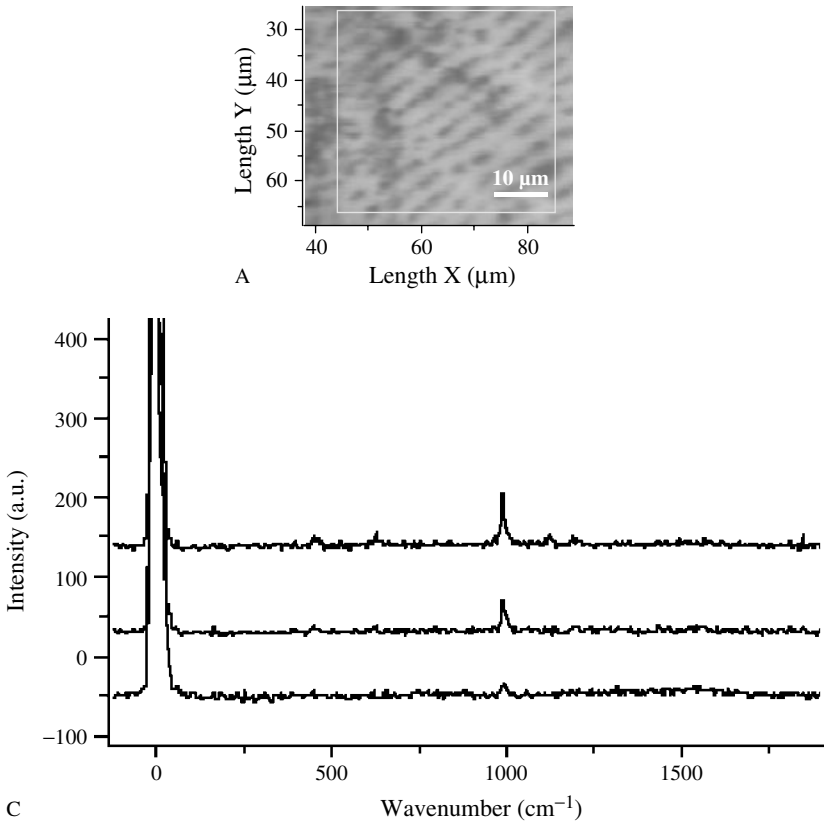

Figure 9. Standard optical microscope picture (A) and Raman mapping (B) of 60 : 40 molar ratio KCl–Na_2SO_4. In this system with a high eutectic melting-point (520 °C), solidified by pushing at a rate of 5 mm h^{-1}, lamellae were clearly visible. The Raman mapping was based on 40 × 40 spectra of the sulfate stretching band in the range 950–1050 cm^{-1}, ratioed over the filtered Rayleigh area from −100 to +100 cm^{-1}. Light areas in (B) contain much sulfate, dark areas only small amounts. Spot size and resolution ~2 μm, obtained with a 50× objective, a 180 μm confocal hole, 100 μm slit width, excited with 200 mW of 514.5 nm radiation for twice per second, averaged and subjected to spike removal. Three examples of Raman spectra with different amounts of sulfate are shown in (C) (abscissa not calibrated). For part (B), see plate 1.

(molar ratio 25 : 75), using the dichromate stretching band at ~850 cm^{-1}, although for this system specimens broke up very easily, probably because of differential contraction on cooling.

Lamellae

Finally, we studied a higher melting eutectic, $KCl–Na_2SO_4$ of molar ratio 60 : 40. For this system, a completely different structure was found, that of parallel lamellae (Fig. 9). This structure we consider to have arisen because the higher melting temperature has given rise to a higher heat flow, which is a necessary condition for the maintenance of a linear solidification front, which in turn allows the formation of lamellae.[13] The way in which lamellar (or fibrous) structures may be formed is indicated in Fig. 10. A planar (linear) front of crystallization is considered important. This requires sufficiently fast heat removal but also time enough for the species (A or B) to diffuse to the appropriate laminae. A high melting-point favours maintenance of a linear front while allowing time for the ions in the salts to diffuse. More comprehensive discussion on the formation of lamellae can be found in a paper by Kerridge[4] and in references cited there.

CONCLUSIONS

In each of the these types of structure, both 'conglomerate' and lamellar, there is a large amount of interfacial contact between the solid solutions with the result that many ions situated at the edge of their phase are also in contact with the neighbouring, but different, structure of the next phase. These ions in non-ideal positions are therefore considered to give rise to the experimental finding of unexpectedly high electrical conductivities which have been found for every salt eutectic so far investigated.[1,2] Since these ions on the edges necessarily have additional energy they give rise to an additional melting enthalpy term.[3,4] In these investigations the solid salt eutectics were cooled at similar rates to those used in this work, and therefore similar solid structures would be expected.

Three groups of workers appear to have published studies on solid salt structures; their photomicrographs show largely lamellar structures for LiF–NaF although one showed a fibrous structure[13,14] and consistently fibrous structures for NaF–NaCl.[13,14] More recent work has shown lamellar structures for $LiF–LnF_3$ (where Ln = La or Pr), fibrous for $LiF–GdF_3$ or a mixture of the two (for Ln = Nd or Sm).[15,16] A lamellar structure was claimed[17] for $PbF_2–ScF_3$. $LiF–CaF_2$ eutectic has also been found to give lamellar structures.[18,19]

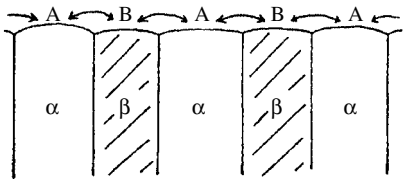

Figure 10. Schematic formation of lamellae (or fibres) on crystallizing an eutectic melt of components A and B. Under suitable unidirectional growth conditions and enough time for diffusion, the melt (top) transforms into the two phases α and β, which constitute the crystal lamellae (bottom).

From this list, it is evident that the systems chosen for study have been somewhat restricted until now, e.g. all the above lamellar systems except one contain LiF, and that it would be of considerable interest to examine a wider range of compounds.

The above discussion indicates that 'conglomerate' structures should generally be expected for lower melting salt eutectics independent of the particular crystallization conditions, but also that lamellar structures can be found with higher melting-point eutectics. We hope to have shown here that these structures can be conveniently studied by Raman microscopy mapping methods.

Acknowledgements

Grateful thanks are expressed to the Danish Technical Science Research Foundation, the Corrit Foundation, the Tuborg Foundation, Danfoss A/S, Thomas B. Thrige Foundation, P. A. Fiskers Foundation and Direktor Ib Henriksen's Foundation for grants which made possible the purchase the DILOR Raman instrument and the 532 nm laser, and also to STVF for a travel grant to D.H.K. and hospitality from DTU. The authors thank Susanne Brunsgaard Hansen of this University for help during preparation of the manuscript.

REFERENCES

1. Eweka EI, Kerridge DH. *Phys. Lett. A* 1993; **174**: 441.
2. Eweka EI. Ph.D. thesis, University of Southampton, 1992.
3. Gaune-Escard M, Kerridge DH. In *Advances in Molten Salts*, Gaune-Escard M (ed.). Begell House: New York, 1999; 270; Gaune-Escard M, Kerridge DH. *High Temp. Mater. Processes* 1999; **3**: 443.
4. Kerridge DH. In *Proceedings of International G. Papatheodorou Symposium*, Boghosian S, Dracopoulos V, Kontoyannis CG, Voyiatis GA (eds). Patras, 1999; 89.
5. Nakamoto K. *Infrared and Raman Spectra of Inorganic and Coordination Compounds*. Wiley-Interscience: New York, 1997; part A, section II.
6. Irish DE, Brooker MH. *Adv. Infrared Raman Spectrosc.* 1976; **2**: 212.
7. Brooker MH. *Can. J. Chem.* 1977; **55**: 1242.
8. Brooker MH. *J. Phys. Chem. Solids* 1978; **39**: 657.
9. Xu K, Chen Y. *J. Raman Spectrosc.* 1999; **30**: 173, 441.
10. Colarusso P, Kidder LH, Levin IW, Lewis EN. In *Encyclopedia of Spectroscopy and Spectrometry*, vol. 3, Lindon JC, Tranter GE, Holmes JL (eds). Academic Press: New York, 1999; 1945.
11. Berg RW, Kerridge DH. *Prog. Molten Salts Chem.* 2000; **1**: 85.
12. Ubbelohde AR. *The Molten State of Matter, Melting and Crystal Structure*. Wiley: Chichester, 1978.
13. Loxham JG, Hellawell A. *J. Am. Ceram. Soc.* 1964; **47**: 184.
14. Cooksey DJS, Munson D, Wilkinson MP, Hellawell A. *Philas. Mag.* 1964; **10**: 745.
15. Trnovcova V, Fedorov PP, Labas V, Starostin MY. In *Solid State Ionics; Science and Technology*, Chowdari BVR (ed.). World Scientific: Singapore, 1998; 325–334.

16. Trnovcova V, Fedorov PP, Barta C, Labas V, Meleshina VA, Sobolev BP. *Solid State Ionics* 1999; **119**: 173.
17. Trnovcova V, Fedorov PP, Buchinskaya IL, Smatko V, Hanic F. *Solid State Ionics* 1999; **119**: 181.
18. Raj SV, Whittenberger JD. *J. Am. Ceram. Soc.* 1990; **73**: 403.
19. Raj SV, Whittenberger JD. *Mater. Sci. Engi. A* 1990; **124**: 113.